EUROFUSION WPJET4-PR(16) 16088

W Helou et al.

ITER-Like Antenna capacitors voltage probes: circuit/electromagnetic calculations and calibrations

Preprint of Paper to be submitted for publication in
Review of Scientific Instruments

This work has been carried out within the framework of the EUROfusion Consortium and has received funding from the Euratom research and training programme 2014-2018 under grant agreement No 633053. The views and opinions expressed herein do not necessarily reflect those of the European Commission.

ITER-Like Antenna capacitors voltage probes: circuit/electromagnetic calculations and calibrations

W. Helou,[1,a)] P. Dumortier,[2,3] F. Durodié,[2] G. Lombard,[1] K. Nicholls,[3] and JET Contributors*

EUROfusion Consortium, JET, Culham Science Centre, Abingdon, OX14 3DB, UK

[1]*CEA, IRFM, F-13108 St-Paul-Lez-Durance, France*

[2]*LPP-ERM/KMS, TEC partner, Brussels, Belgium*

[3]*CCFE, Culham Science Centre, Abingdon, OX14 3DB, UK*

The analyses illustrated in this manuscript have been performed in order to provide the required data for the amplitude-and-phase calibration of the D-dot voltage probes used in the ITER-like Antenna at the Joint European Torus tokamak. Their equivalent electrical circuit has been extracted and analyzed, and it has been compared to the one of voltage probes installed in simple transmission lines. A Radio-Frequency calibration technique has been formulated and exact mathematical relations have been derived. This technique mixes in an elegant fashion data extracted from measurements and numerical calculations to retrieve the calibration factors. The latter have been compared to previous calibration data with excellent agreement proving the robustness of the proposed Radio-Frequency calibration technique. In particular, it has been stressed that it is crucial to take into account environmental parasitic effects. A Low-Frequency calibration technique has been in addition formulated and analyzed in depth. The equivalence between the Radio-Frequency and Low-Frequency techniques has been rigorously demonstrated. The Radio-Frequency calibration technique is preferable in the case of the ITER-like Antenna due uncertainties on the characteristics of the cables connected at the inputs of the voltage probes. A method to extract the effect of a mismatched data acquisition system has been derived for both calibration techniques. Finally it has been outlined that in the case of the ITER-like Antenna voltage probes can be in addition used to monitor the currents at the inputs of the antenna.

I. INTRODUCTION

The Ion Cyclotron Resonance Frequency (ICRF) antenna called ITER-Like Antenna (ILA) at the Joint European Torus (JET) tokamak is an array of 8 electrically-short loops denoted as straps arranged in 2 toroidal by 2 poloidal array of Resonant Double Loops (RDL). Each RDL is in arrangement of two poloidally adjacent straps fed through vacuum matching capacitors from a common Vacuum Transmission Line. Details about the ILA, its impedance matching and operation can be found in Ref. 1-2. The ILA is equipped with 16 voltages probes. They are used to monitor the complex voltages at the 8 straps inputs. At each strap input, 2 voltage probes are used at the same reference plane for redundancy reasons. The measured voltages are used to control the phases of the straps voltages, to protect the matching capacitors from possible over-voltage, over-current and over-heating, and assess the quality of the chosen impedance matching in terms of distribution of the voltages across the 8 straps.

[a)] Author to whom correspondence should be addressed. Electronic mail: walid.helou@cea.fr.

*See the Appendix of F. Romanelli et al., Proceedings of the 25th IAEA Fusion Energy Conference 2014, Saint Petersburg, Russia

The measured voltages are also used as an input for the so-called Scattering Matrix Arc Detection (SMAD) system[3].These sixteen voltage probes have to be calibrated, in both amplitude and phase.

The manuscript is organized as follows. In a first section, a voltage probe installed in a transmission lines is studied. In a next section, the ILA capacitors voltages probes are analyzed in depth; their equivalent circuit is introduced, and their behavior is assessed using full-wave electromagnetic calculations and Radio-Frequency (RF) network computations. In a third section, the so-called "dummy capacitor" is introduced. In a fourth section, the RF calibration is analyzed in detail, and exact mathematical relations are derived. Full-wave and RF network computations are performed and mixed with measured data to extract the calibration factors. In a fifth section, the Low-Frequency (LF) calibration is studied in detail and compared to the RF calibration. Finally the manuscript ends by a conclusion and some final remarks. The reported full-wave electromagnetic calculations are performed using ANSYS HFSS®, and the RF network calculations using SIDON[4,5] network solver. Note that care has been taken to properly normalize the S-matrices at all ports when using SIDON[4,5].

II. A VOLTAGE PROBE IN A TRANSMISSION LINE

A voltage probe installed in a transmission line (Fig.1a) can be considered as a capacitive voltage divider[6,7], and its equivalent electric circuit is illustrated in Fig.1b. Its transfer function can be easily extracted, as in (1) where a harmonic time variation (e^{+jwt}) is considered. In Fig. 1 and (1), C_1 is the coupling capacitance between the voltage at the probe's input (V_{probe}) and the main transmission line's voltage just below the probe ($V_{electrode}$). C_2 is the capacitance between the probe's tip and its ground. $Z_{probe}=R_{probe}+jX_{probe}$ is the load impedance at the probe's input (it is the impedance of the data acquisition system Z_{DAQ} transformed by the transmission line(s) connecting it to the probe).

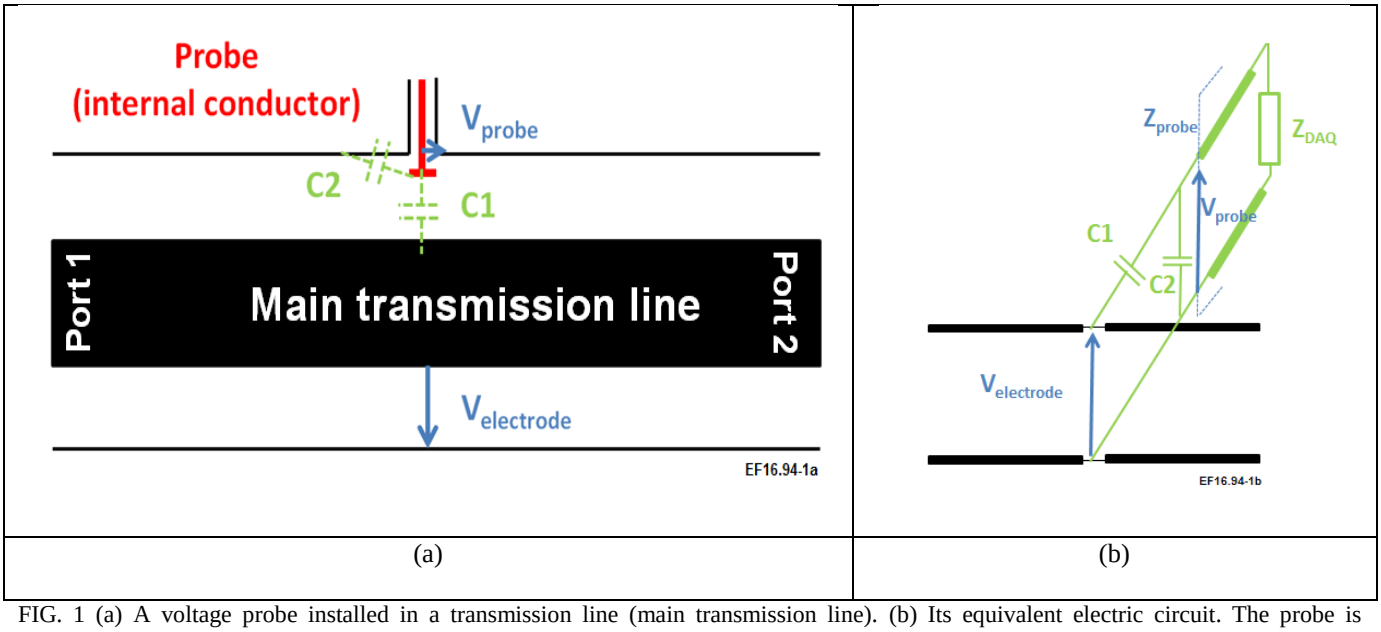

(a) (b)

FIG. 1 (a) A voltage probe installed in a transmission line (main transmission line). (b) Its equivalent electric circuit. The probe is connected to the data acquisition system (DAQ) by a cable.

$K_{v,probe} = \frac{V_{electrode}}{V_{probe}} = \frac{1 + jZ_{probe}(C_1 + C_2)w}{jZ_{probe}C_1 w}$	(1a)
$K_{v,probe} = \frac{1}{jZ_{probe}C_1 w} \qquad if \qquad \lvert Z_{probe}\rvert(C_1 + C_2)w \ll 1$	(1b)
$K_{v,probe} = 1 + \frac{C_2}{C_1} \qquad if \qquad \lvert Z_{probe}\rvert(C_1 + C_2)w \gg 1$	(1c)

From (1), one distinguishes two extreme modes of operation[6,7] of a voltage probe:

- D-dot mode (1b), where D refers to the electric displacement field (B-dot is the analog mode for current probes). It is the case of sufficiently low frequencies. In time domain, the probe performs a proportional time-derivative of the time-varying voltage below the probe (for harmonic signals the latter one is $V_{electrode}e^{jwt}$, and its derivative is simply $jwV_{electrode}e^{jwt}$). In frequency domain, the phase of $K_{v,probe}$ is -90° minus the phase of Z_{probe} (i.e. constantly -90° if Z_{probe} is real), and its amplitude decreases by 20 dB/decade if Z_{probe} is frequency independent. Note that here $K_{v,probe}$ is independent from C_2, but the value of Z_{probe} (and thus Z_{DAQ}, and the effect of the transmission line(s) connecting the probe to the data acquisition system) is of a high importance since here $K_{v,probe}$ is inversely proportional to Z_{probe}. This means that any error on Z_{probe} directly affects $K_{v,probe}$ since $1/(1+\alpha) \sim 1 - \alpha + O(\alpha)$.
- Self-integrating mode (1c). In time domain, the probe's time-varying voltage has its amplitude proportional to the time-varying voltage just below the probe. In frequency domain, for all frequencies, the ratio between the voltages is constant and both voltages are in phase. Note that here $K_{v,probe}$ is independent from Z_{probe}.

In frequency domain, (1b) and (1c) are the asymptotes of (1a). For harmonic voltages, it seems that one can operate the probe in either self-integrating or D-dot mode, but one shall stress the dependence of $K_{v,probe}$ on Z_{probe} in the D-dot mode. In the ILA, the voltage probes are operated in their D-dot mode. This also the case of the voltage probes in the ICRF antennas of the W-Tungsten Environment in Steady-state Tokamak (WEST)[8]. However it seems that in some other ICRF antennas the probes are operated in the self-integrated mode[9].

III. VOLTAGE PROBES IN THE ILA

In the ILA, the voltage probes are installed at the top and bottom of the matching capacitors as illustrated in Fig.2a (i.e. not in a homogenous transmission line section). Fig.2b illustrates the ANSYS HFSS® model of an ILA's matching capacitor installed in its housing (i.e. the ground). Ports 1 and 2 correspond respectively to the matching capacitors so-called variable and fixed electrodes where the latter is connected to a strap. Ports 3 and 4 correspond to the voltage probes inputs and correspond respectively to the TOP and BOTTOM probes for capacitors $C_{matching,i}$ with i=1…4, and to the BOTTOM and TOP probes for capacitors $C_{matching,i}$ with i=5…8. Note that all ports have been conveniently de-embedded so as to be compatible with the RF network computations of Ref. 2. Fig. 3a illustrates a longitudinal cut-view of the ANSYS HFSS®

model of an ILA matching capacitor installed in its housing. The matching capacitor's cylinders are explicitly sketched, as well as its alumina ceramic. It can be easily demonstrated that the RF problem of the matching capacitor with its two probes can be split into two decoupled RF problems where each problem is a matching capacitor and a single probe, however the mathematical demonstration has been omitted here for brevity. Fig.3b illustrates the equivalent electric circuit of the latter problem if one neglects in a first order the matching capacitor's self-inductance.

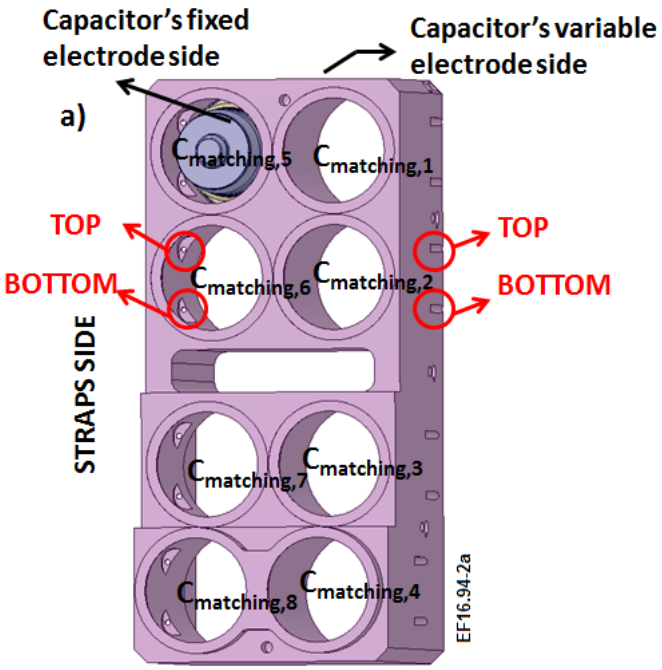

(a)

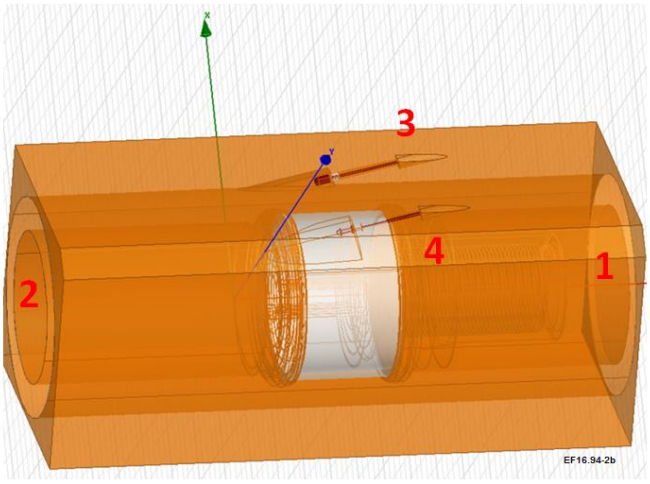

(b)

FIG. 2 (a) Voltage probes in the ILA. The red circles illustrate the emplacement of the voltage probes at the TOP/BOTTOM of each matching capacitor. (b) ANSYS HFSS® model of an ILA matching capacitor and its voltage probes.

In Fig. 3, notations of Fig.1 have been adopted. As usual, a capacitance C_2 (~1.6 pF) is present between the probe's tip and its ground; however two probes coupling capacitances are present here: C_1=C_{1f} (~50 fF) and C_{1v} (~5 fF). The latter are the coupling capacitances between the voltage at the probe's input (V_{probe}) and the voltages at matching capacitors fixed ($V_{electrode}$=$V_{electrode,f}$) and variable electrodes ($V_{electrode,v}$) respectively.

After some algebra, one easily finds (2), where one readily retrieves the D-dot and the self-integrating regimes in (2b) and (2c). Note that in the latter equation C_{1v} has been neglected when compared to C_2. One shall notice the similarity of these equations with (1b) and (1c). In (2) one shall stress the appearance of $\alpha_{disturb}$.

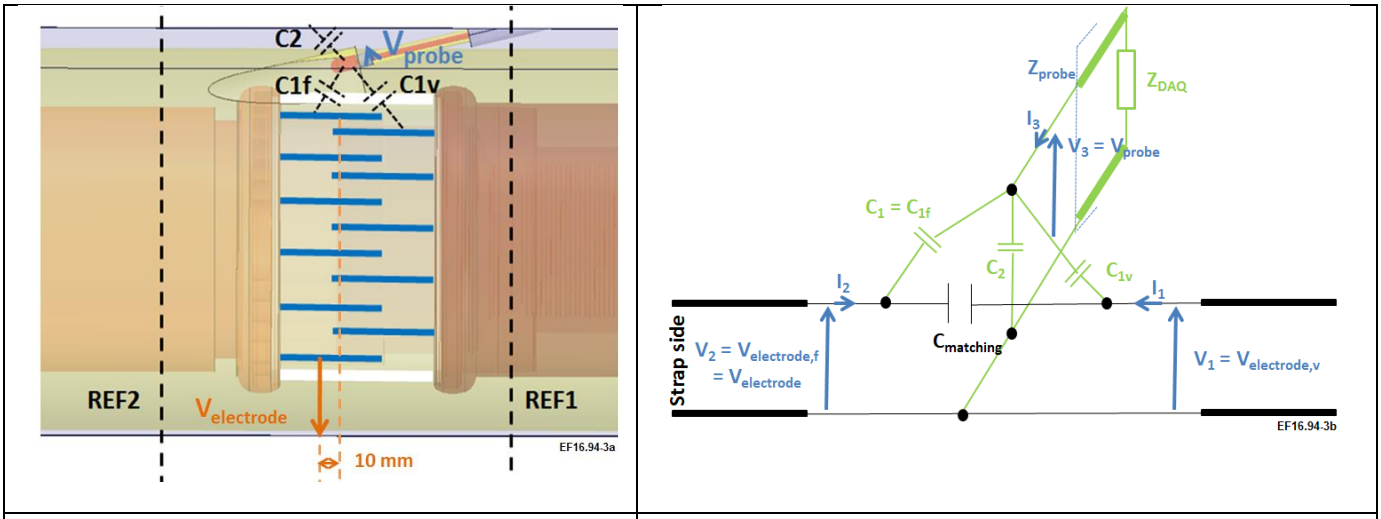

(a) (b)

FIG. 3 (a) Longitudinal cut-view of the ANSYS HFSS® model of an ILA matching capacitor with its voltage probes (one probe is seen in this cut-view). REF1 and REF2 indicate the reference planes of the ANSYS HFSS® model at ports 1 and 2. The capacitor's alumina ceramic is in white. The position of $V_{electrode}$ is illustrated (b) The equivalent electric circuit of a voltage probe and its environment in the ILA. The black filled circles indicate branch-nodes.

$$K_{v,probe} = \frac{V_{electrode}}{V_{probe}} = \frac{1 + jwZ_{probe}(C_1 + C_{1v} + C_2)}{jwZ_{probe}C_1} \overbrace{\frac{1}{1 + \frac{C_{1v}}{C_1}\frac{V_{electrode,v}}{V_{electrode}}}}^{\alpha_{disturb}} \quad (2a)$$

$$K_{v,probe} = \frac{1}{jZ_{probe}C_1 w}\alpha_{disturb} \qquad if \qquad |Z_{probe}|(C_1 + C_{1v} + C_2)w \ll 1 \quad (2b)$$

$$K_{v,probe} = (1 + \frac{C_2}{C_1})\alpha_{disturb} \qquad if \qquad |Z_{probe}|(C_1 + C_{1v} + C_2)w \gg 1 \quad (2c)$$

At this point one shall stress that C_{1v} is around 10% of C_1 as found using electrostatic calculations performed on FEMM open source software (http://www.femm.info/wiki/HomePage). Also, the value of $|V_{electrode,v}|$ do not exceed 30% of $|V_{electrode}|$ in the operation conditions of the ILA (i.e. around a matching point), this can be seen in Fig. 4a. Hence, $K_{v,probe}$ of (2) can be replaced by $K_{v,probe}$ of (1), independently from the values of the voltages at matching electrodes (i.e. from the strap's impedance, matching capacitor's value and input power). The error due to the latter approximation shall be of the order of 0.1x30<5%. Note that the latter observation is valid whatever the frequency is. This is sketched in Fig.4b

Note that, as illustrated in Fig. 3a, V_{probe} is the voltage at the probe's input. Concerning $V_{electrode}$, since in the ANSYS HFSS® model the voltage at the reference plane REF2 (see Fig. 3a) is not exactly $V_{electrode}$ of Fig. 3b (due to a non-homogenous transmission line section), some assessment has been performed to obtain the proper location of $V_{electrode}$.. It has been found to be 10 mm away from the position just below the probe tip, as illustrated in Fig. 3a. A quadrupole (called "de-

embedding quadrupole" in what follows) relating the voltages and currents at REF2 (V_2 and I_2) and those at the position of $V_{electode}$ ($V_{electrode}$ and $I_{electrode}$) has been simulated on ANSYS HFSS®. Details of this assessment are omitted here for brevity.

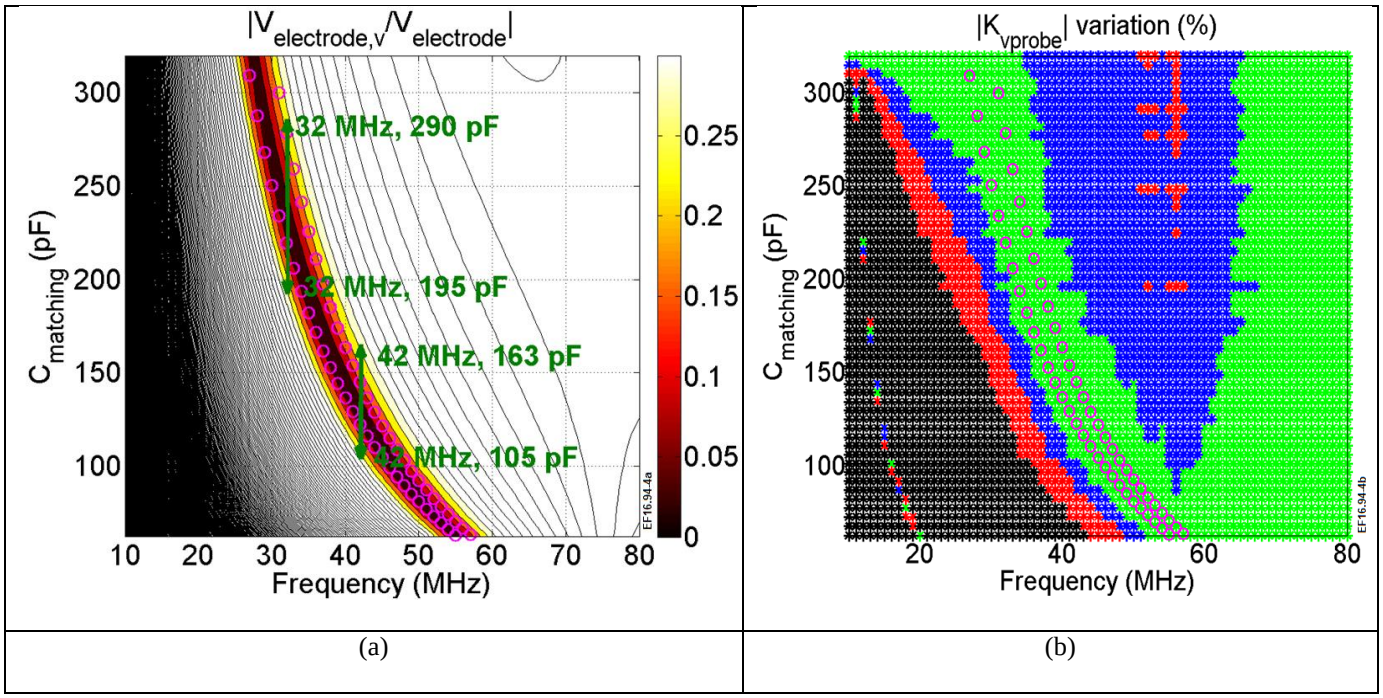

FIG. 4 (a) 2D scan of $|V_{electrode,v}/V_{electrode}|$ as function of the frequency and the value of the matching capacitor. Magenta circles illustrate, at each frequency, a couple of capacitors (C_{m1} and C_{m2}) required at matching. (b) Variation (in percent) of $|K_{vprobe}|$ from its value considered for a matching capacitance equal to $(C_{m1}+C_{m2})/2$ at each frequency. Green, blue, red and black symbols correspond respectively to regions with $|K_{vprobe}|$ variations of less than 5, 5 to 10, 10 to 20 and more than 20 percent.

To cross-check that $K_{v,probe} = V_{electrode}/V_{probe}$ is constant all along the plasma shot, regardless of the high variation of the straps S-matrix when transiting from so-called Low to High plasma confinement modes[10] (and vice-versa) and during Edge Localized Modes[11], "ICRF plasma shots" with a WEST ICRF antenna have been simulated using SIDON[4,5] at various frequencies and with ILA matching capacitors as matching elements. The fact that WEST ICRF antennas have been modeled instead of the ILA has absolutely no impact on the analysis (WEST ICRF antennas and ILA have very similar RF circuits). Fig.5 summarizes the calculation results obtained all along the simulated plasma shots at 27, 35, 48, 52.5, 55 and 57 MHz. The y-axes in Fig. 5b, d, f and h are the maximum relative errors from the mean values obtained at each frequency. One concludes from Fig. 5 that $\alpha_{disturb}$ of (2) is indeed of the order of 1+/-0.05.

Note that due to the specificity of a strap's impedance, $Z_{strap} = R_{strap}+jX_{strap}$, where X_{strap} is almost constant at a given frequency and $X_{strap} >>> R_{strap}$, $I_{electrode}$ can be extracted from the probes measurements with a relatively small error (see Fig. 5f,h), in addition to $V_{electrode}$. This can be explained using (3) where Z_{probe} is usually 50 Ω and ζ is almost constant at a given frequency f_0. The 40 dB/decade slope in Fig. 5e and the almost constant ~-180° of $K_{i,probe}$ in Fig. 5g can be also understood from (3). Since no electrical current sensors are installed at the inputs of the straps, the latter observation can be used as a

fast-security current measurement by simply dividing the measured voltage by the straps reactance extracted from modeling. Note that monitoring the currents at the straps inputs is mandatory for the matching capacitors safety, in particular avoiding their overheating. The mentioned technique can be useful despite the small variation of the straps reactance during an increase of the plasma edge electron density[12] as during Edge Localized Modes[13].

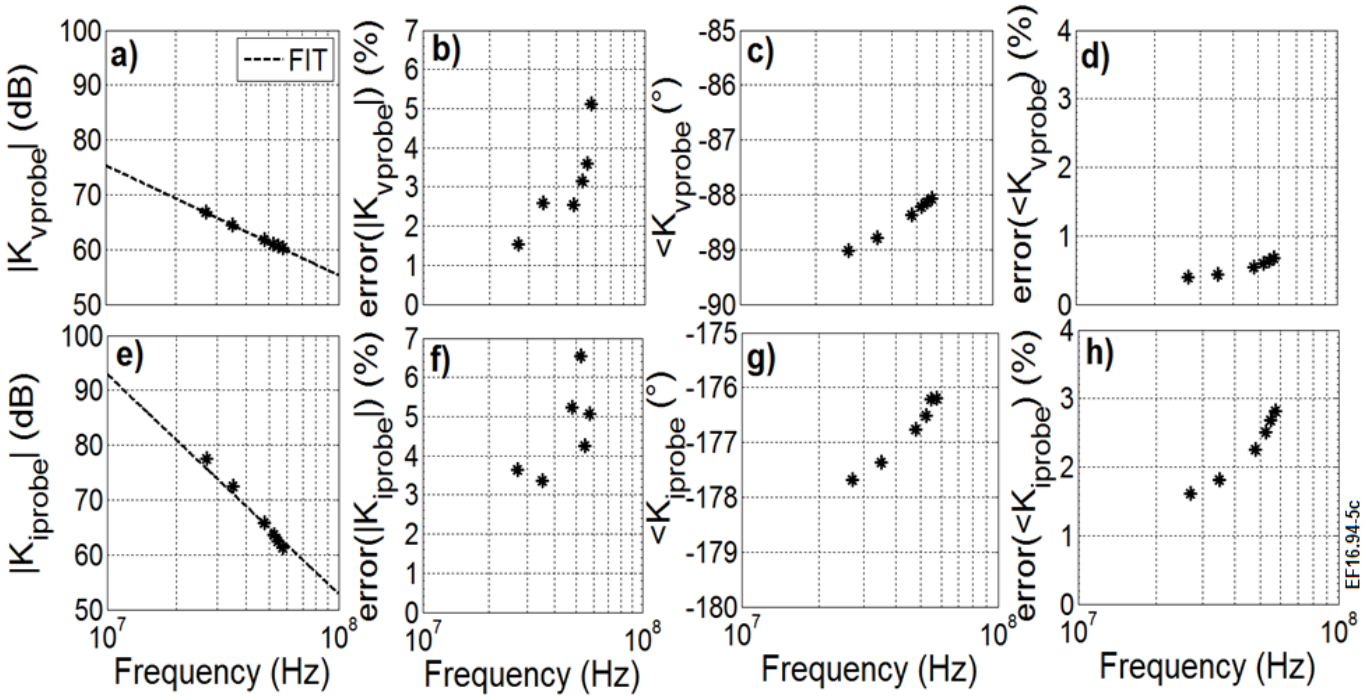

FIG. 5. (a,c,e,g) The amplitude and phase of $K_{v,probe} = V_{electrode}/V_{probe}$ and $K_{i,probe} = I_{electrode}/I_{probe}$ at various frequencies (b,d,f,h) Corresponding relative errors at each calculated frequency. I_{probe} is the current at the position of V_{probe}. The 20 and 40 dB/decade fits in subplots (a) and (e) are extrapolated from $|K_{v,probe}|$ and $|K_{i,probe}|$ at 48MHz. For instance, the extrapolation gives $|K_{v,probe}|$ = 62.93 dB at 42MHz.

$$K_{i,probe} = \frac{I_{electrode}}{I_{probe}} = \frac{V_{electrode}/Z_{electrode}}{V_{probe}/Z_{probe}} = Z_{probe}\frac{K_{v,probe}}{Z_{electrode}}$$	(3a)
$$Z_{electrode} \sim R_{strap} + jX_{strap} \sim jX_{strap} \sim j\zeta 2\pi f_0$$	(3b)

IV. THE DUMMY CAPACITOR

The calibration of the ILA's voltage probes is performed using a so-called dummy capacitor. This component has the same external shape as the ILA matching capacitors but it includes only the external cylinders of the fixed and variable electrodes. The dummy capacitor and the ILA matching capacitors have the same ceramic, and they are fabricated by the same manufacturer so as to reduce the discrepancies. Fig. 6a sketches a schematic of the calibration setup and Fig. 6b illustrates a picture of the dummy capacitor. The latter is installed inside the housing of the so-called bridge, and is drove towards the housing of a matching capacitor where it is mechanically connected to a strap through an insulating guide flange made from polyamide material. One shall stress that there is no DC electrical contact between the fixed electrode of the dummy capacitor and the strap. Since it has been demonstrated that the voltage at the variable electrode side barely affects

$K_{v,probe}$, the variable electrode side of the dummy capacitor is short-circuited (i.e. connected to the housing through an RF contact). The fixed electrode side is excited by an RF-cable mounted through a tube which passes through the bridge. The reference planes (REFi, i=1…3) where the Vector Network Analyzer (VNA) is connected are indicated by dashed vertical lines in Fig. 6a. The VNA has been calibrated accordingly to these reference planes. Port1 (corresponding to pseudo-waves a_1 and b_1) is connected to the dummy capacitor's fixed electrode at REF1, ports 2 and 3 (corresponding to pseudo-waves a_2 and b_2, and a_3 and b_3 respectively) are connected to the TOP and BOTTOM voltage probes respectively at REF2 and REF3. $V_{electrode}$, $V_{probe,1}$, $V_{probe,2}$, $Z_{probe,1}$ and $Z_{probe,2}$ are as defined in Fig. 3 and are illustrated in Fig.6a. Due to the Thermocoax and RG223 cables, the additional variables are used in what follows: $V_{probe,ref,1}$, $V_{probe,ref,2}$, $Z_{probe,ref,1}$ and $Z_{probe,ref,2}$.They are respectively, the voltages at the reference planes of the VNA ports 2 and 3 and the impedances connected later-on to these ports. Note that the Thermocoax and RG223 cables characteristics are not precisely known. The dummy capacitor has been modeled on ANSYS HFSS® (in addition to the de-embedding quadrupole enabling the retrieval of the voltages and currents 10 mm below the probes tips), and the resulting S-matrices have been used in SIDON network calculations. The K_{vprobe} factors obtained from network calculations of the dummy capacitor are identical to those of voltage probes installed in the matching capacitors.

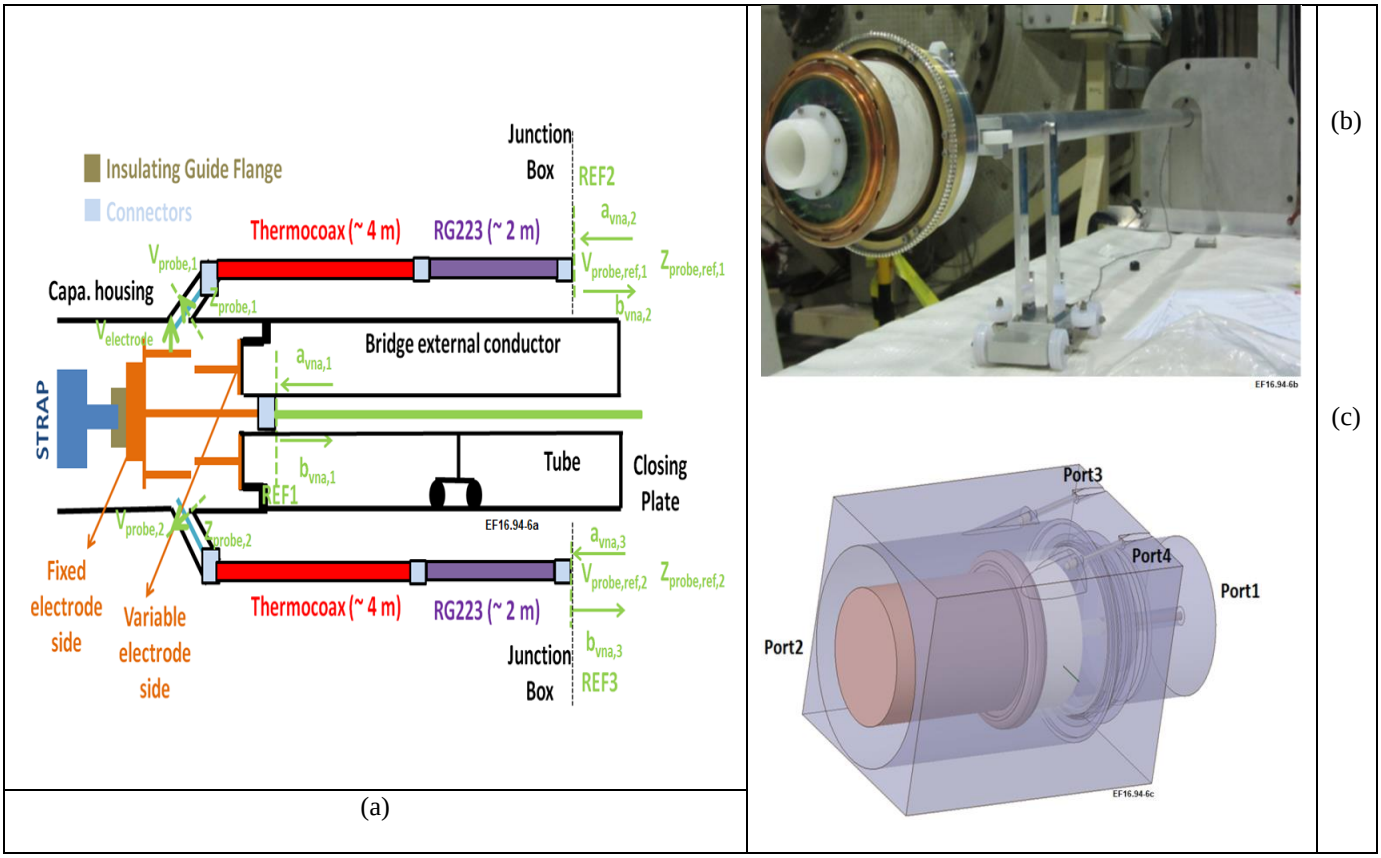

FIG. 6. (a) Schematic of the voltage probes calibration using the new dummy capacitor. (b) Picture of the dummy capacitor. The insulating guide flange is seen at the left-side of the figure. (c) 3D view of the octopole representing the dummy capacitor simulated on ANSYS HFSS®.

V. RADIO-FREQUENCY CALIBRATION

A. Problem formulation

The aim of the RF calibration[14] is to extract $K_{v,probe,ref,} = V_{electrode}/V_{probe,ref}$ for the TOP and BOTTOM voltage probes at each ILA matching capacitor. One connects the dummy capacitor to the strap S_i, i=1…8 (each strap Si corresponds to $C_{matching,i}$) through the insulating guide flange. The 4x4 S-matrix of the dummy capacitor (S_{dummy}) of Fig. 6c connected to an impedance Z_{load} (a strap cascaded with an insulating guide flange) at its port 2 reduces to a 3x3 matrix that is measured by the VNA (S_{vna}). Indeed, ports 1, 3 and 4 of S_{dummy} correspond respectively to ports 1, 2 and 3 of the measured S_{vna}. A this point, one shall set equation (4) where $\Gamma_{ref,i}=a_{vna,i}/b_{vna,i}$ (i=2,3) and $R_{ref,vna}$ =50 Ω.

From (4), one understands that two classes of coefficients are required to extract the factor $K_{v,probe,ref,i}$:

a) Coefficients extracted from modeling, namely the dimensionless factor K_{HFSS}. In order to extract K_{HFSS}, one can simulate the dummy capacitor of Fig. 6c in ANSYS HFSS® and connect it in SIDON to arbitrary loads at its ports 3 and 4 (for instance 50 Ω) and an arbitrary excitation at port 1 (for instance 1 W of incident power). The impedance connected at its port 2, Z_{load}, shall however be set to a proper value (see section V.B). From the latter simulations, $V_{electrode}$ is computed and then K_{HFSS} is simply extracted using (4g).

b) Coefficients extracted from measurements. Namely $S_{vna,21}$, $S_{vna,31}$, $S_{vna,22}$, $S_{vna,33}$, $\Gamma_{ref,2}$ and $\Gamma_{ref,3}$. One understands that no a priori knowledge of the Thermocoax and RG223 characteristics is required; their effect is inherently taken into consideration by the RF measurements. Note that $\Gamma_{ref,i}$ = 0 only when the probes are connected to the VNA at REF2 and REF3, but not necessarily when the probes are connected to the data acquisition system. $Z_{probe,ref,1}$ and $Z_{probe,ref,2}$ of (4a,b) are simply the impedances seen from the so-called junction box at REF2 and REF3 (see Fig. 6a) when looking towards the data acquisition system. Note that the latter is connected to the junction box by ~80 m RF cables. The mismatch of the data acquisition system can be easily taken into account by injecting measured values of $\Gamma_{ref,2}$ and $\Gamma_{ref,3}$ in (4e) and (4f). It shall be stressed that for $\Gamma_{ref,2}$ and $\Gamma_{ref,3}$ even as low as ~-35dB in amplitude, the calibration factors remain uncertain to +/- 4% in amplitude and +/- 2°in phase if the measured values of $\Gamma_{ref,2}$ and $\Gamma_{ref,3,}$ are not taken into account. In the case of the ILA voltage probes, it has been decided to set $\Gamma_{ref,2}$ and $\Gamma_{ref,3}$ to zero instead of their real values (~-35dB in amplitude).

Note that $S_{vna,21}$, $S_{vna,31}$ depend on the geometry of the dummy capacitor, Z_{load}, and the geometry of the probes and their surroundings (i.e. C_{1f}, C_{1v} and C_2 of Fig. 3). $S_{vna,22}$ and $S_{vna,33}$ depend on the geometry of the probes and their surroundings, while K_{HFSS} depends on the geometry of the dummy capacitor and $Z_{load.}$ It is worthwhile to mention that calculations have

been performed to assess the impact of relative permittivity of the matching capacitors and the dummy capacitors alumina ceramic on the voltage probes calibration. It showed to have a minor impact.

$$Z_{probe,ref,1} = R_{ref,vna}\frac{1+\Gamma_{ref,2}}{1-\Gamma_{ref,2}}$$	(4a)
$$Z_{probe,ref,2} = R_{ref,vna}\frac{1+\Gamma_{ref,3}}{1-\Gamma_{ref,3}}$$	(4b)
$$b_{vna,2} = S_{vna,21}a_{vna,1} + S_{vna,22}a_{vna,2} + \overbrace{S_{vna,23}}^{\to 0}a_{vna,3} = S_{vna,21}a_{vna,1} + S_{vna,22}\Gamma_{ref,2}b_{vna,2}$$ $$\to \left(1 - S_{vna,22}\Gamma_{ref,2}\right)b_{vna,2} = S_{vna,21}a_{vna,1}$$ $$\to \frac{V_{probe,ref,1}}{\sqrt{R_{ref,vna}}} = a_{vna,2} + b_{vna,2} = \left(1+\Gamma_{ref,2}\right)b_{vna,2} = \frac{1+\Gamma_{ref,2}}{1-S_{vna,22}\Gamma_{ref,2}}S_{vna,21}a_{vna,1}$$	(4c)
$$\frac{V_{probe,ref,2}}{\sqrt{R_{ref,vna}}} = a_{vna,3} + b_{vna,3} = \left(1+\Gamma_{ref,3}\right)b_{vna,3} = \frac{1+\Gamma_{ref,3}}{1-S_{vna,33}\Gamma_{ref,3}}S_{vna,31}a_{vna,1}$$	(4d)
$$K_{v,probe,ref,1} = \frac{V_{electrode}}{V_{probe,ref,1}} = \frac{V_{electrode}}{a_{vna,1}}\frac{a_{vna,1}}{V_{probe,ref,1}} = \frac{K_{HFSS}}{S_{vna,21}}\frac{1-S_{vna,22}\Gamma_{\mathrm{ref,2}}}{1+\Gamma_{\mathrm{ref,2}}}$$	(4e)
$$K_{v,probe,ref,2} = \frac{V_{electrode}}{V_{probe,ref,2}} = \frac{V_{electrode}}{a_{vna,1}}\frac{a_{vna,1}}{V_{probe,ref,2}} = \frac{K_{HFSS}}{S_{vna,31}}\frac{1-S_{vna,33}\Gamma_{\mathrm{ref,3}}}{1+\Gamma_{\mathrm{ref,3}}}$$	(4f)
$$K_{HFSS} = \frac{V_{electode}}{a_{vna,1}\sqrt{R_{ref,vna}}}$$	(4g)

B. Effect of Z_{load} and parasitic effect of the insulating guide flange

Fig. 7a illustrates the circuit analyzed in this section. The dummy capacitor of Fig.6c, is connected at its port 2 to an impedance $Z_{load}=R_{ref,vna}(1+S_2)/(1-S_2)$. Since $|S_{ji}|$ has been found to tend to zero $\forall$ i$\in$[1,4]-{j} for j = 3 and 4 (i.e. the ports corresponding the voltage probes), the electrical signals at ports 1 and 2 can be properly analyzed while simply ignoring the presence of ports 3 and 4. The S-matrix, S, characterizing the interaction between ports 1 and 2 is simply S_{dummy} minus its lines 3 and 4, and columns 3 and 4. One sets equation (5), where V_2, I_2, A and B are respectively the voltages and currents at the port 2 of the dummy capacitor, and the elements of the first line of the chain matrix of the de-embedding quadrupole relating V_2 and I_2 to the voltages and currents at the position of $V_{electrode}$ (see Fig. 3a). It is evident from (5f) that K_{HFSS} is

defined not only by the geometry of the dummy capacitor, but also by Z_{load}. As an example, Fig. 7b illustrates $|K_{HFSS}|$ at 42 MHz for various loads $Z_{load} = |Z_{load}| \exp(j\Phi_{Zload})$ where Φ_{Zload} is the phase of Z_{load}.

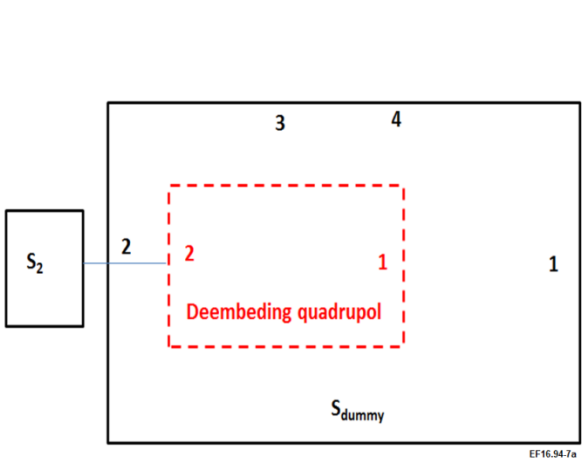

(a)

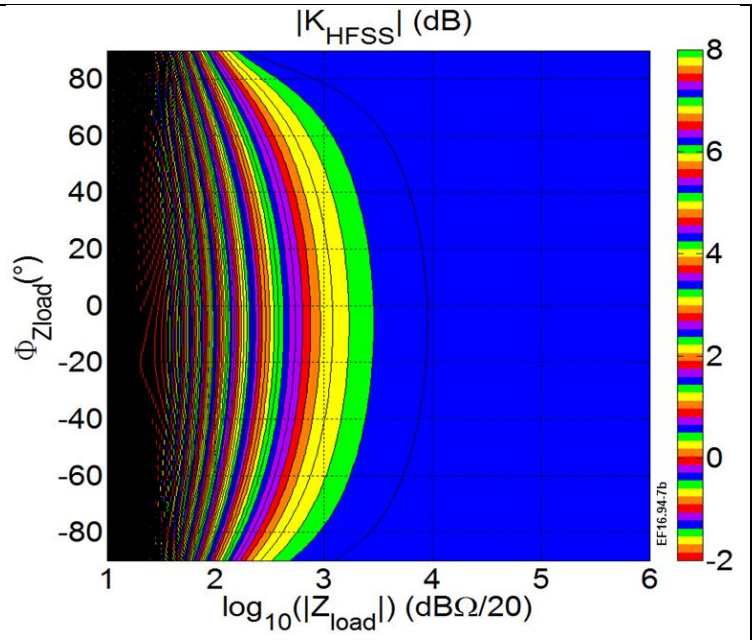

(b)

FIG. 7. (a) Block diagram of the dummy capacitor of Fig.6c connected at its port 2 to an impedance $Z_{load}=R_{ref,vna}(1+S_2)/(1-S_2)=|Z_{load}| \exp(j\Phi_{Zload})$. The internal quadrupole indicated with red dashed lines is the de-embedding quadrupole that enables to retrieve the voltages and currents 10 mm below the probes tips. (b) Amplitude in dB of K_{HFSS} for various loads Z_{load} at 42 MHz (a similar plot can be obtained for the phase of K_{HFSS}).

One concludes from the figure above, that K_{HFSS} is almost constant for high $|Z_{load}|>10^4$ Ω. This observation means that it is highly desirable to have high $|Z_{load}|$, since in this case the measured values of $S_{vna,i}$ and the calculated value of K_{HFSS} can be mixed in confidence to extract $K_{v,probe,ref,i}$ (i=2,3) without the need of a precise knowledge of the (complex) value of Z_{load}. However, in an opposite case of low $|Z_{load}|$, an exact knowledge of $|Z_{load}|$ and Φ_{Zload} is required. At this stage, if one considers the insulating guide flange as being equivalent to a simple series stray capacitance $C_{insul,parasitic}$, and if one neglects the straps impedance and replaces it by a simple short-circuit, Z_{load} would be equivalent to $1/jC_{insul,parasitic}w$ (w being the angular frequency). By setting the condition $|Z_{load}|>10^4$ Ω, and by considering a frequency of 50 MHz (~highest operation frequency of the ILA), one finds the requirement $C_{insul,parasitic}<320$fF. Unfortunately, full-wave calculations of the insulating guide flange illustrated that it is equivalent to a stray capacitance of around 20 pF, which is by two order of magnitudes higher that 320 fF. The final model of the dummy capacitor thus includes the insulating guide flange (see Fig. 8a), and Z_{load} is taken to be equal to a strap's reactive impedance (see Fig. 8b) extracted from TOPICA[15] simulations of the ILA antenna.

$a_2 = S_2 b_2$	(5a)
$b_2 = \frac{S_{21}}{1 - S_{22}S_2} a_1$	(5b)

$V_2 = (a_2 + b_2)\sqrt{R_{ref,vna}}$	(5c)
$I_2 = (a_2 - b_2)/\sqrt{R_{ref,vna}}$	(5d)
$V_{electrode} = AV_2 - BI_2$	(5e)
$K_{HFSS} = \left[A(S_2 + 1) - \frac{B}{R_{ref,vna}}(S_2 - 1)\right] \frac{S_{21}}{1 - S_{22}S_2}$	(5f)

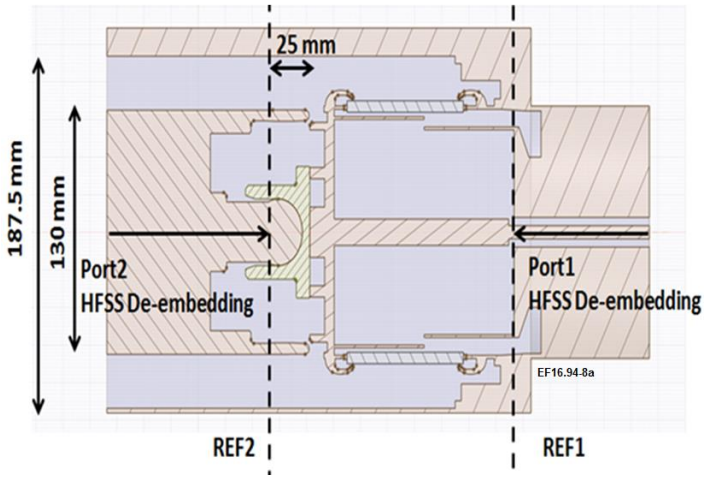

(a)

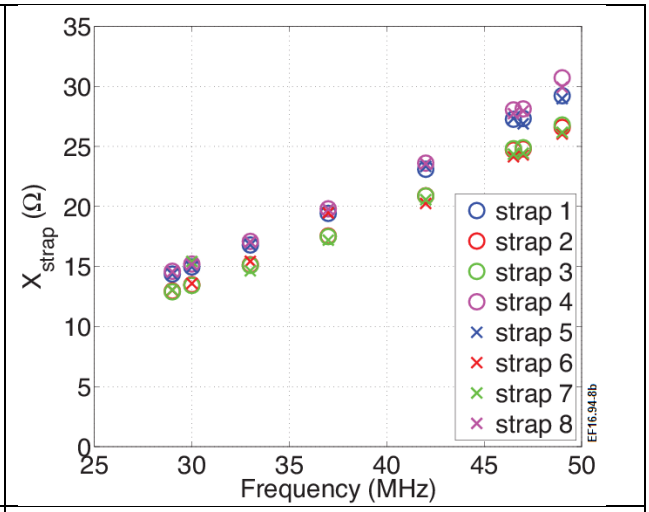

(b)

FIG. 8. (a) Accurate model of the dummy capacitor including the insulating guide flange. (b) The straps reactances extracted from ILA Z-matrices obtained from TOPICA.

C. K_{HFSS} extraction

The extraction of K_{HFSS} is performed using the dummy capacitor of Fig. 8a and $Z_{load} = jX_{strap}$ where X_{strap} is the one Fig. 8b. The latter has been available at discrete frequencies (29, 30, 33, 37, 42, 46.5, 47 and 49 MHz), K_{HFSS} has thus been extracted at first at these discrete frequencies. Since the dielectric constant of the dummy capacitor's insulating guide flange is unknown, 3 values have been considered: 3, 3.5 and 4 (a lossless material has been assumed). Note that to retrieve $V_{electrode}$ 10mm away from the voltage probes tips, a de-embedding quadrupole has been calculated for each permittivity case. Thus 24 values of K_{HFSS} have been extracted at each discrete frequency (8 straps x 3 values of the polyamide dielectric constant). The computed 24 values being all in the range of +/- 1.5% in amplitude and +/- 1.5 ° in phase from the mean value, the latter has been considered as the value of K_{HFSS} for all the 8 straps. A simple polynomial fitting has then been employed in order to retrieve the value of K_{HFSS} for any frequency in the [29 - 49] MHz interval. This is illustrated in Fig. 9. A technique has been also implemented to extrapolate K_{HFSS} outside the range [29 - 49] MHz but details are omitted here for brevity.

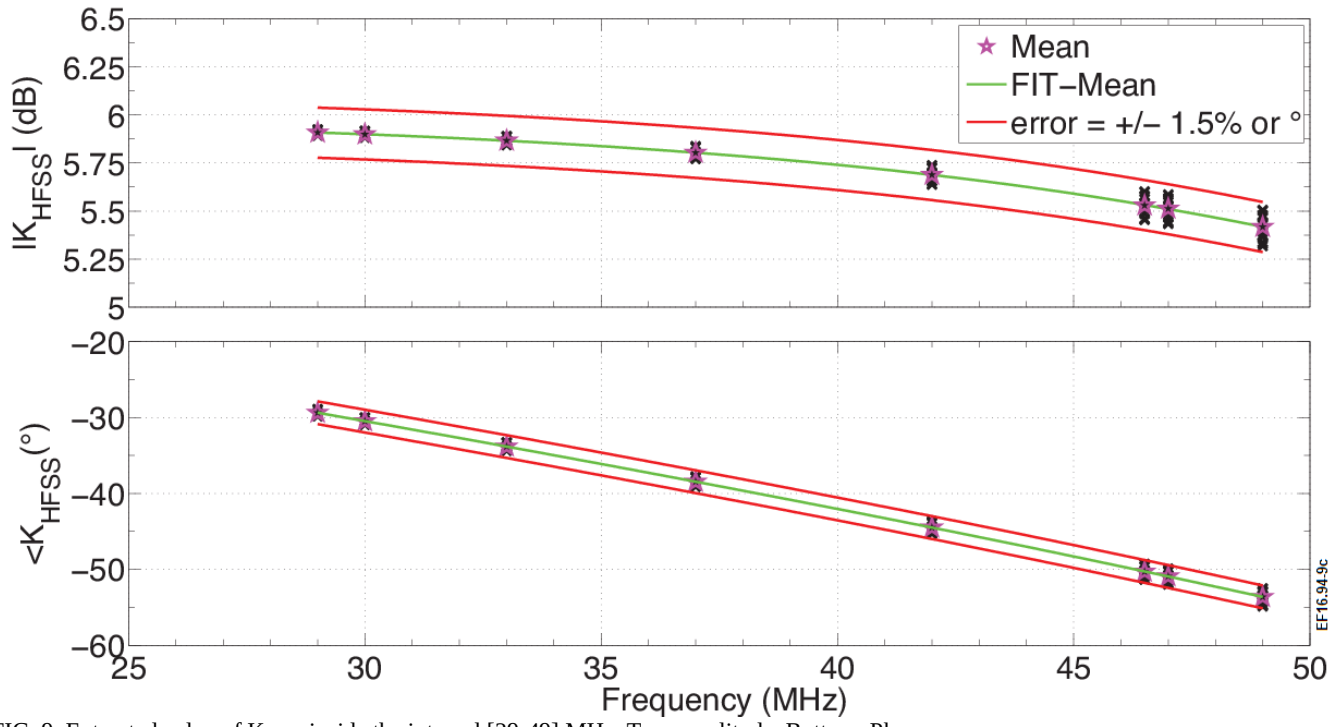

FIG. 9. Extracted value of K_{HFSS} inside the interval [29-49] MHz. Top: amplitude. Bottom: Phase.

D. The 7mm offset

For the voltage probe calibration the dummy capacitor assembly is positioned such that the dummy capacitor flange is fully pushed against the antenna strap flange sub-assembly. The Vacuum Transmission Line (VTL) assembly of the ILA during operations however is positioned such that the dummy capacitor flange is retracted by 7 mm from the antenna strap flange sub-assembly in order to provide compliance for thermal expansion of the VTL assembly. This is done by acting at the rear of the antenna by retracting the VTL flange with respect to the antenna main square flange. The 7 mm offset is illustrated in Fig.10. Since the VNA measurements and the illustrated K_{HFSS} factor calculations have been performed with a 0 mm offset of the dummy capacitor, and the final position of the matching capacitor corresponds to the 7 mm offset case, the value of $K_{v,probe,ref}$ needs a final correction due to the latter offset using (6). In the latter equation, $K_{v,probe,ref,i}$ is the calibration factor that shall be used to compute the voltage at the matching capacitor fixed electrode using the voltage at the probe. K_{HFSS} is as extracted in section V.C, i.e. with the insulating guide flange taken into account (Fig. 8a) and a zero offset. $S_{vna,21}$, $S_{vna,31}$, $S_{vna,22}$ and $S_{vna,33}$ are measured values (with a zero offset of the dummy capacitor) and $\Gamma_{ref,2}$ and $\Gamma_{ref,3}$ are here set to zero. $K_{v,probe,ref,i,offset=0mm,Zload=10k\Omega}$ is a simulated value of the calibration factor with a 0 mm offset and a dummy capacitor of Fig. 6c, $K_{v,probe,ref,i,offset,Zload=10k\Omega}$ is the same as $K_{v,probe,ref,i,offset=0mm,Zload=10k\Omega}$ but with a non-zero offset. Calculations show that a 7 mm offset decreases the value of the calibration factor by 7% in amplitude without impacting its phase.

$$K_{v,probe,ref,1} = \frac{K_{HFSS}}{S_{vna,21}} \frac{1 - S_{vna,22}\Gamma_{\mathrm{ref},2}}{1 + \Gamma_{\mathrm{ref},2}} K_{offset}$$	(6a)
$$K_{v,probe,ref,2} = \frac{K_{HFSS}}{S_{vna,31}} \frac{1 - S_{vna,33}\Gamma_{\mathrm{ref},3}}{1 + \Gamma_{\mathrm{ref},3}} K_{offset}$$	(6b)
$$K_{offset} = mean(K_{offset,1}\ ;\ K_{offset,2})$$	(6c)
$$K_{offset,i} = \frac{K_{v,probe,ref,i,offset,Zload=10k\Omega}}{K_{v,probe,ref,i,offset=0mm,Zload=10k\Omega}}\ , i = 1,2$$	(6d)

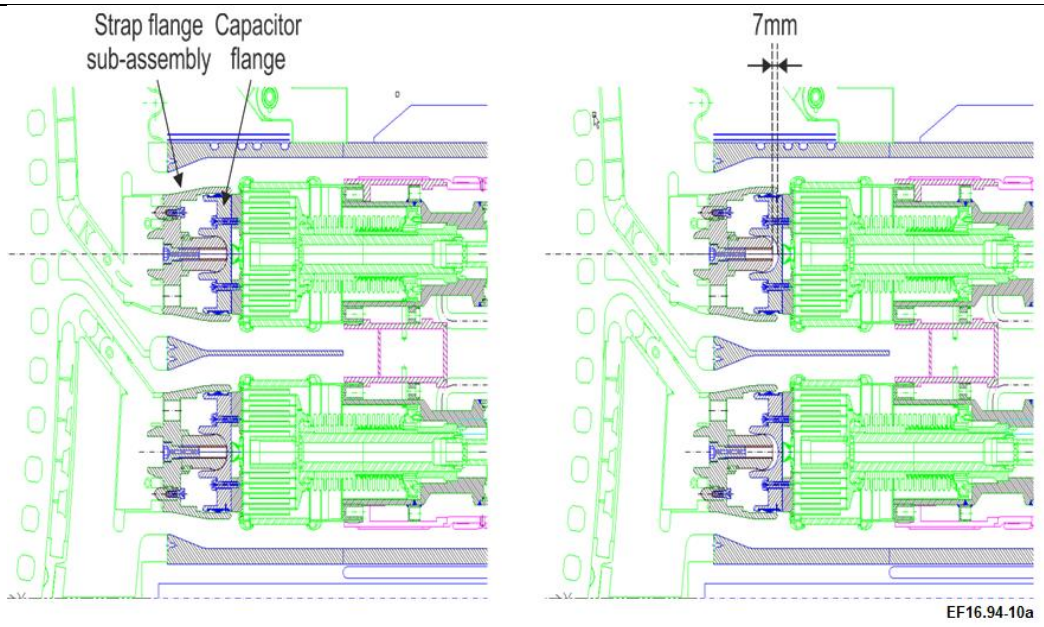

(a)

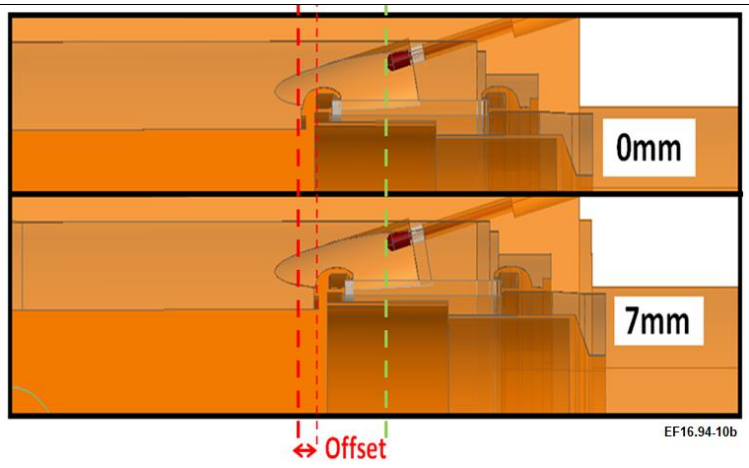

(b)

FIG. 10. The 7mm offset. (a) Left: ILA capacitor flange pushed against the antenna strap flange sub-assembly (position used for the voltage probe calibration). Right: ILA capacitor flange retracted by 7mm (ILA operation position). (b) Impact of the VTL offset on the capacitor's position with respect to the voltage probes. The dashed green line illustrates the position of the voltage probes tips. The thick red dashed line represents the position of the capacitor's corona ring extremity with a 0 mm offset, and the thin red dashed line its position with the 7 mm offset.

E. Calibration

Fig. 11 illustrates the resulting calibration factor at the TOP voltage probe of the ILA matching capacitor 1 (CAP1). Similar results have been obtained for the TOP and BOTTOM probes of all other capacitors. The crucial effect of the insulating guide flange (stray capacitance) is clearly seen. Neglecting it for frequencies above 35 MHz implies huge errors of much more than +/- 10% or °. The resonances appearing above 70 MHz are attributed to the self-resonances of the LC tank formed by the strap, the insulating guide flange the dummy capacitor and all stray elements. Very good agreement is obtained with the calibration factors extracted in 2008 employing another type of dummy capacitor and a more direct calibration method[16] (the latter has not been employed in the new calibrations due to access restriction). The data of the curve "Final Interpol" is now implemented in the ILA data acquisition system.

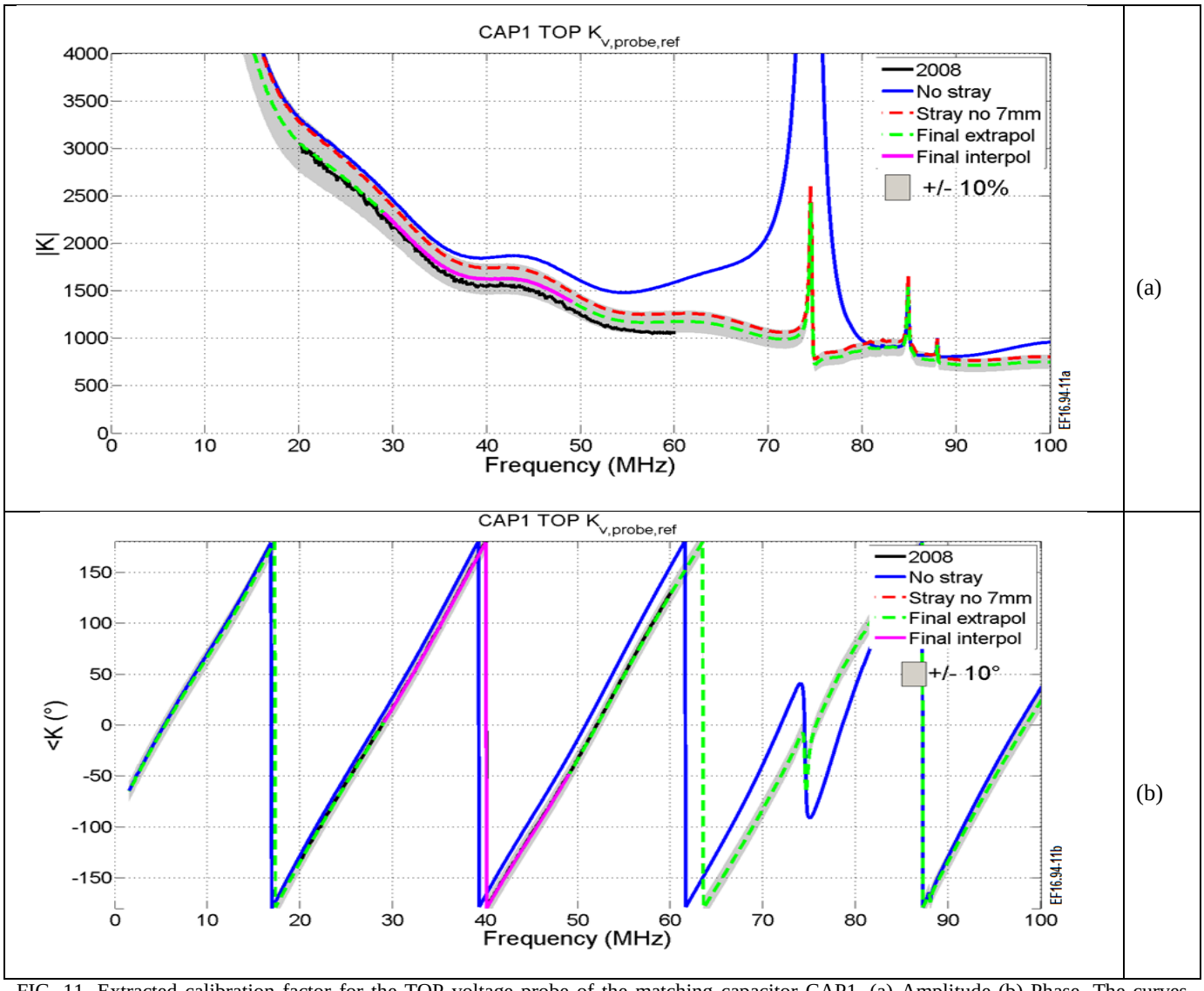

FIG. 11. Extracted calibration factor for the TOP voltage probe of the matching capacitor CAP1. (a) Amplitude (b) Phase. The curves correspond to data extracted in 2008[16] (curve "2008"), without taking into account the effect of the insulating guide flange nor the 7 mm offset (curve "No stray"), without taking into account the 7 mm offset but considering the effect of the insulating guide flange (curve "Stray no 7 mm"), data using (6) (extrapolation and interpolation, curves "Final extrapol" and "Final interpol" respectively). Details about the extrapolation have been omitted for brevity.

VI. LOW-FREQUENCY CALIBRATION

A. Problem formulation

This calibration is denoted as "Low Frequency" (LF) technique since it relies on extrapolating the calibration factor $K_{v,probe,ref}$ at the ICRF frequency range (20-60 MHz) from extracted values at low frequencies (< 1 to few MHz). This is done by assuming a D-dot operation regime of the voltage probes. At this stage one shall consider equation (7) where the A and B are the elements of the first line of the chain matrix of the equivalent vacuum-filled transmission line of length D_{eq} and characteristic impedance Z_{0eq} connected to a voltage probe ($A=\cosh(\gamma D_{eq})$ and $B = Z_{0eq}\sinh(\gamma D_{eq})$. γ is the propagation constant of the latter transmission line. In (7a), a D-dot regime is assumed; $V_{electrode}/V_{probe}$ is given by (1b). After some algebra, (7a) reduces to (7b) with all variables considered at a frequency f_i except the assumed frequency independent parameters C_1 and D_{eq}.

$$K_{v,probe,ref} = \frac{V_{electrode}}{V_{probe,ref}} = \frac{V_{electrode}}{V_{probe}}\frac{V_{probe}}{V_{probe,ref}} = \frac{1}{jZ_{probe}C_1 w}\left(A + \frac{B}{Z_{probe,ref}}\right) = \frac{1}{jC_1 w}\frac{1}{Z_{0eq}\frac{Z_{probe,ref}+Z_{0eq}\tanh(\gamma D_{eq})}{Z_{0eq}+Z_{probe,ref}\tanh(\gamma D_{eq})}}\left(\cosh(\gamma D_{eq}) + \frac{Z_{0eq}}{Z_{probe,ref}}\sinh(\gamma D_{eq})\right)$$	(7a)
$$K_{v,probe,ref,fi} = \frac{1}{jZ_{probe,ref,fi}C_1 w_{fi}}\left(\cosh(\gamma_{fi} D_{eq}) + \frac{Z_{probe,ref,fi}}{Z_{0eq,fi}}\sinh(\gamma_{fi} D_{eq})\right)$$	(7b)

By considering $K_{v,probe,ref}$ at two frequencies f_1 and f_2, one obtains (8) where the following assumptions have been considered:

- Z_{0eq} is frequency independent and real.
- The equivalent vacuum-filled transmission line is lossless ($\gamma_{f2} \rightarrow j2\pi f_2/c$).
- $Z_{probe,ref,f1} = R_{ref,vna}$ (the reference impedance of the VNA).
- f_1 is a very low frequency, this implies: $\cosh(\gamma_{f1}D_{eq})\rightarrow 1$, $\sinh(\gamma_{f1}D_{eq})\rightarrow 0$, and $V_{electrode,f1}\rightarrow V_{vna,1,f1}$ (the voltage at REF1, see Fig. 6a).

$$K_{v,probe,ref,f2} = K_{v,probe,ref,f1}\ \frac{f_1}{f_2}\ \frac{R_{ref,vna}}{Z_{probe,ref,f2}}\left[\cos(2\pi f_2 D_{eq}/c) + j\frac{Z_{probe,ref,f2}}{Z_{0eq}}\sin(2\pi f_2 D_{eq}/c)\right]$$	(8a)
$$K_{v,probe,ref,f1} = \frac{V_{electrode,f1}}{V_{probe,ref,f1}} \cong \frac{V_{vna,1,f1}}{V_{vna,2,f1}} = \frac{(a_{vna,1,f1} + b_{vna,1,f1})\sqrt{R_{ref,vna}}}{(a_{vna,2,f1} + b_{vna,2,f1})\sqrt{R_{ref,vna}}} = \frac{1 + S_{vna,11,f1}}{S_{vna,21,f1}}$$	(8b)

From (8), the LF calibration is clear: using $S_{vna,11}$ and $S_{vna,21}$ measured at low frequency, one extrapolates the value of the calibration factor at any frequency in the voltage probe's D-dot mode. The effect of $Z_{probe,ref}$ and the equivalent transmission

line connected to the voltage probe can be easily taken into account. $Z_{probe,ref,f2}$ can be simply measured using the VNA, and the characteristics of the transmission line shall be known *a priori* or somehow extracted.

The following additional observations can be made:

- If $Z_{probe,ref} = Z_{0eq} = R_{ref,vna}$, the amplitude of $K_{vprobef,ref2}$ is inversely proportional to the frequency (D-dot mode), and its phase is the one of $K_{vprobef,ref1}$ but shifted by the phasor $\exp(j2\pi f_2 D_{eq}/c)$ due to the transmission line length.

- If $D_{eq} = 0$, (8a) reduces to $K_{v,probe,ref,f2} = K_{v,probe,ref,f1} \times f_1/f_2 \times R_{ref,vna}/Z_{probe,ref,f2}$.
If in addition $Z_{probe,ref,f2} = R_{ref,vna}$, one retrieves $K_{v,probe,ref,f2} = K_{v,probe,ref,f1}\ f_1/f_2$.

- Suppose $K_{v,probe,ref,f2}=K_{v,probe,ref,R}$ has been extracted using $Z_{probe,ref,f2} = R_{ref,vna} = R$, it can be observed that the extraction of $K_{v,probe,ref,Z}$ for $Z_{probe,ref,Z} = Z$ at the same frequency f_2 using (9) is fully equivalent to the correction using $(1-S_{vna,ii}\Gamma_{ref,i})/(1+\Gamma_{ref,i})$ in (4e,f). This is illustrated in the appendix.

$$\frac{K_{v,probe,ref,Z}}{K_{v,probe,ref,R}} = \frac{R}{Z}\ \frac{\cosh(\gamma D_{eq}) + \frac{Z}{Z_{0eq}}\sinh(\gamma D_{eq})}{\cosh(\gamma D_{eq}) + \frac{R}{Z_{0eq}}\sinh(\gamma D_{eq})} \qquad (9)$$

B. Calibration

The Thermocoax and RG223 cables (see Fig. 6a) equivalent vacuum length have been extracted using measured data. This extraction is not detailed for brevity. Note however that the equivalent characteristic impedance remained unknown. The dummy capacitor's S-parameters have been measured at 27 discrete frequencies between 300 kHz and 500 kHz. Thus, for each probe the calibration factor is considered as the average value of 27 extrapolations performed using (8). As an example, Fig. 12 illustrates the results of a LF calibration for the TOP probe of $C_{matching1}$ for a cables equivalent characteristic impedance of $Z_{0eq} = 45\ \Omega$. Superimposed is the RF calibration factor, as well as a +/- 10% or ° margin from the RF calibration.

Note that in this section the LF calibration does not include the correction due to the 7 mm offset of section V.D and the RF calibration of Fig. 12 corresponds to the curve "Stray no 7mm" of Fig. 11a. The discrepancy between the RF and LF curves of Fig. 12 are most likely due to the uncertainty on the characteristics of the transmission lines connected to the probe. Still one can conclude that with an accurate knowledge of the cables characteristics, the LF and RF techniques are fully equivalent.

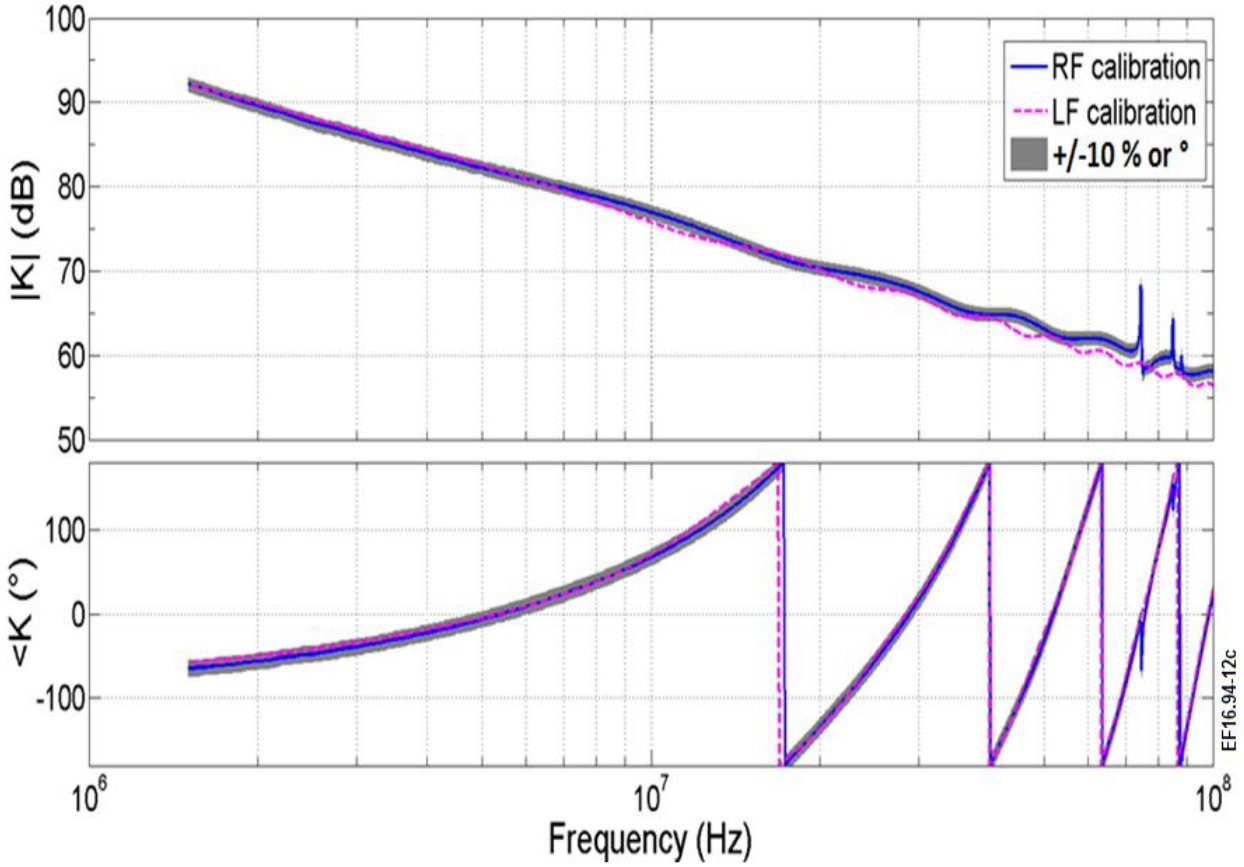

FIG. 12. RF and LF calibration factor for the TOP probe of the matching capacitor 1. The LF calibration is considered with Z_{0eq} = 45 Ω. One can notice that at very low frequencies the RF and LF curves are superimposed as one would expect.

VII. CONCLUSION

This manuscript illustrates a rigorous analysis of D-dot voltage probes and their calibration. The equivalent circuit of a voltage probe in a simple transmission line has been first analyzed, and then the ILA voltage probes have been studied in depth. A simple technique for measuring the currents at the straps has been outlined. It relies on the fact that the straps impedance is almost reactive and independent, at a first order, from the plasma configuration. This technique can be implemented for instance as a fast security FPGA measurement to monitor the capacitors current and protect them from overheating. The RF calibration technique has been rigorously studied, and exact mathematical relations have been derived. This RF technique mixes in an elegant fashion data from measurements and numerical calculations to retrieve the calibration factors. The technique proved to be robust and precise despite the use of uncommon RF components (the dummy capacitor). It has been outlined that it is crucial to take into account environmental parasitic effects, specifically when employing components with considerable dimensions. Indeed, it has been seen that considering the effect of the insulating guide flange is critical for a proper RF calibration. The LF calibration technique has been analyzed in depth, and detailed mathematical relations have been formulated taking into account transmission lines at the input of the probes. The equivalence between the RF and LF calibration techniques has been rigorously demonstrated and a method to take into account a mismatched data

acquisition system (DAQ) has been derived for both techniques. It has been stressed that even a very well matched DAQ (up to -35 dB), might add a few percent error on the calibration factors, if not taken into account. A concluding remark might be drawn when comparing the RF and LF calibration methods: Due to the unknown characteristics of the Thermocoax and RG223 cables, the RF calibration technique might be preferred in the case of the ILA voltage probes. In a case where a direct access to the voltage probes input is possible, one might prefer the LF calibration technique since it avoids mixing measured data with data extracted from numerical computations. Note that, as for any numerical calculation, the latter is prone to errors due to meshing, convergence, etc. A final comment shall be made: it is advisable to always terminate an unused probe, or the cable(s) to which it is connected, by a matched load; this might avoid cavity modes (leading to arcing and overheating) between the probe's tip and the load – details are out of scope of this manuscript.

ACKNOWLEDGMENTS

The authors would like to thank the team of K. Nicholls from CCFE for their technical support in performing the calibrations. This work has been carried out within the framework of the EUROfusion Consortium and has received funding from the Euratom research and training programme 2014-2018 under grant agreement No 633053. The views and opinions expressed herein do not necessarily reflect those of the European Commission.

APPENDIX

The appendix demonstrates the equivalence between (4e,f) and (9). Equation (A1) is (4e) but with the subscripts "vna" and "ref" omitted for simplicity. In (A1), $K_{v,probe,ref}$ is considered for $\Gamma = (Z-R)/(Z+R)$ where $R = R_{ref,vna}$. In (A2), Z has been replaced by R (hence $\Gamma=0$). Equation (A3) is simply the ratio between (A2) and (A1).

$$K_{v,probe,ref} = \frac{K_{HFSS}}{S_{21}} \frac{1 - S_{22}\Gamma}{1 + \Gamma} = K_{v,probe,ref,Z}$$	(A1)
$$K_{v,probe,ref,R} = \frac{K_{HFSS}}{S_{21}}$$	(A2)
$$\frac{K_{v,probe,ref,Z}}{K_{v,probe,ref,R}} = \frac{1 - S_{22}\Gamma}{1 + \Gamma}$$	(A3)

One can readily perform (A5).

$$\frac{1-S_{22}\Gamma}{1+\Gamma} = \frac{1-\frac{G-Y_{0eq}th(\gamma D_{eq})}{G+Y_{0eq}th(\gamma D_{eq})}\frac{G-Y}{G+Y}}{1+\frac{G-Y}{G+Y}}$$
$$= \frac{\left(G+Y_{0eq}th(\gamma D_{eq})\right)(G+Y)-\left(G-Y_{0eq}th(\gamma D_{eq})\right)(G-Y)}{2G\left(G+Y_{0eq}th(\gamma D_{eq})\right)}$$
$$= \frac{Y+Y_{0eq}th(\gamma D_{eq})}{G+Y_{0eq}th(\gamma D_{eq})} = \frac{\frac{1}{Z}+\frac{1}{Z_{0eq}}\frac{sinh(\gamma D_{eq})}{cosh(\gamma D_{eq})}}{\frac{1}{R}+\frac{1}{Z_{0eq}}\frac{sinh(\gamma D_{eq})}{cosh(\gamma D_{eq})}}$$
$$= \frac{R}{Z}\frac{\cosh(\gamma D_{eq})+\frac{Z}{Z_{0eq}}\sinh(\gamma D_{eq})}{\cosh(\gamma D_{eq})+\frac{R}{Z_{0eq}}\sinh(\gamma D_{eq})} \quad \text{(A4)}$$

In (A4), the following notations have been used: G=1/R, Y=1/Z, $Y_{0eq}=1/Z_{0eq}$. Note that $\Gamma=(Z-R)/(Z+R)=(G-Y)/(G+Y)$, and $S_{22}=(G-Y_{0eq}th(\gamma D_{eq}))/(G+Y_{0eq}th(\gamma D_{eq}))$, where $Y_{0eq}th(\gamma D_{eq})$ is the admittance of the probe (considered here as an ideal open-circuit) transformed by the transmission line of length D_{0eq}, characteristic impedance Z_{0eq} and propagation constant γ.

REFERENCES

[1]F. Durodié, et al., Plasma Phys. Control. Fusion 54 (2012) 074012.
[2]F. Durodié, et al., AIP Conf. Proc. 1689, 070013 (2015).
[3]M. Vrancken, et al., Fusion Eng. Des. 84 (2009) 1953–1960.
[4]W. Helou, et al., IEEE 2015 9th European Conference on Antennas and Propagation (EuCAP), Lisbon, Portugal, 12-17 April 2015.
[5]W. Helou, et al., AIP Conf. Proc. 1689, 070004 (2015).
[6]P. Choi, et al., Tenth IEEE International Pulsed Power Conference, 1995, Albuquerque, NM, USA, pp. 880-885, vol 2.
[7]S. Won Lim, et al., IEEE Transactions On Plasma Science, vol. 41, no. 10, October 2013.
[8]W. Helou, et al., Fusion Eng. Des. 96–97 (2015) 473–476.
[9]I. Stepanov, et al., Fusion Eng. Des. 88 (2013) 990– 993.
[10]F. Wagner et al., Phys. Rev. Lett. 49, 1408 (1982).
[11]H. Zohm, Plasma Phys. Control. Fusion 38 (1996) 105–128.
[12]A. Messiaen, et al., Plasma Physics and Controlled Fusion, Vol. 31, No. 6. pp. 921 to 939, 1989.
[13]I. Monakhov, et al., AIP Conf. Proc. 694, 2003, pp. 146–149.
[14]P. Dumortier, et al., AIP Conf. Proc. 1689, 070003 (2015).
[15]V. Lancellotti, et al., Nucl. Fusion 46 (2006) S476–S499.
[16]M. Vrancken, et al., Fusion Eng. Des. 82 (2007) 873–880